Chinese Chemical Letters 33 (2022) 4400–4404

Contents lists available at ScienceDirect

Chinese Chemical Letters

journal homepage: www.elsevier.com/locate/cclet

Unusual hexa-nuclear cadmium cluster functionalized phosphomolybdate as effective photoelectrochemical sensor for trace Cr(VI) detection

Wenting An, Xiujuan Zhang, Jiaqi Niu, Yuanyuan Ma*, Zhangang Han*

Hebei Key Laboratory of Organic Functional Molecules, National Demonstration Center for Experimental Chemistry Education, College of Chemistry and Materials Science, Hebei Normal University, Shijiazhuang 050024, China

ARTICLE INFO

Article history:
Received 13 November 2021
Revised 6 December 2021
Accepted 10 December 2021
Available online 18 December 2021

Keywords:
Phosphomolybdate
Cadmium cluster
Photoelectrocatalysis
Electrochemical detection
Hexavalent chromium

ABSTRACT

Photo-assisted electrochemical technique provides a promising approach towards carcinogen chromium(VI) detection, which requires reasonable catalyst design. Herein, an unusual hexa-nuclear cadmium cluster functionalized reductive phosphomolybdate hybrid as photo-electrochemical sensor was designed and synthesized with formula of $\{[Cd(H_2O)_2]_2[Cd(btmbp)]_2\}\{Cd(P_4Mo_6O_{31}H_7)_2\}\cdot 20H_2O$ (**1**) (btmbp= 4,4′-bis((1*H*-1,2,4-triazol-1-yl)methyl)biphenyl), in which the photoactive hexa-nuclear $\{Cd_6\}$ clusters cooperated with reductive phosphomolybdate $[P_4Mo_6O_{31}]^{12-}$ endow the material with wide light absorption and remarkable redox activity, thus achieving efficient photo-assisted electrochemical Cr(VI) detection performance. Under visible-light assistance, the detection limit (LOD) and sensitivity of Cr(VI) is 4.17 nmol/L (0.225 ppb) and 226.32 μA L/μmol, which is apparently superior to the performance without photo-assistance (6.25 nmol/L and 106.95 μA L/μmol) and far satisfies the demands of world health organization (WHO) for potable water (50 ppb). Moreover, compound **1** showed prominent Cr(VI) detection performance in practical water samples together with remarkable anti-interference capacity and good electrochemical durability. This work provides an important guidance for designing efficient polyoxometalate-based crystalline sensors for Cr(VI) detection.

Heavy metal contamination brings out severe environmental intimidation to human health as a result of their biotoxicity and amassing in human body [1–3]. Hexavalent chromium, denoted as Cr(VI), as a representative of high poisonous heavy-metal contaminants has attracted the widespread attention of many researchers because of its high carcinogenic-mutagenic effect and poisonousness on human body [4–7]. Nowadays, the Cr(VI)-containing species have been included in the human carcinogen set by International Agency for Research on cancer (IARC) and World Health Organization (WHO) and the maximum permissible limit for total Cr content in potable water and industrial water are 0.05 ppm and 0.5 ppm [8,9], respectively. Therefore, establishing an efficient and rapid detection approach to achieve the effective monitor on Cr(VI) content is very significant and urgency.

At present, electrochemical sensing methods have been widely known as a reliable analytic approach for detecting Cr(VI) with trace level due to their inherent merits including simple operation, high sensitivity, short analysis time and low detection limit [10–13]. During the electrochemical detection process, Cr(VI) pollutants can be transformed into non-toxic Cr(III) species *via* a direct electron-transfer pathway to produce an obvious analytical signal for the quantitative detection. To facilitate the electron transfer and achieve more efficient electrochemical detection, external field-assistance strategy (light, heat, *etc.*), has been considered as one of effective approaches, among which photo-assistance exhibit promising application in electrochemical detection due to its green and environment-friendly feature [14–16]. Si *et al.* constructed surface-engineered MI-TiO_2/ITO electrode and achieved efficient photo-assisted electrochemical detection of bisphenol A in water with wide detection range, high sensitivity and good renewability [17]. Hu *et al.* reported zeolitic imidazolate framework-8 electrode achieved effective electrochemical detection of organic pollution under the light illumination with lower detection limitation and superior regeneration property [18]. The photogenerated electron on electrochemical sensors could synergistically accelerate the electron transfer process [19], thus enhancing the detection performance. Therefore, it is expected that employing photo-assisted strategy in electrochemical Cr(VI) detection will achieve

* Corresponding authors.
E-mail addresses: mayy334@hebtu.edu.cn (Y. Ma), hanzg116@hebtu.edu.cn (Z. Han).

https://doi.org/10.1016/j.cclet.2021.12.021
1001-8417/

the improvement on electrochemical performance but rarely reported so far.

To achieve effective photo-assisted electrochemical detection, the reasonable design of electrochemical sensor with suitable photocatalytic activity is crucial adjective. Polyoxometalates (POMs), as a distinctive and intriguing category of nanosized anionic metal-oxo clusters, have displayed enormous application potential in various fields owing to their structural diversity and fascinating physicochemical properties [20–25]. Among POMs family, hourglass-type phosphomolybdate $\{M[P_4Mo^V{}_6O_{31}]_2\}^{n-}$ (abbr. $M\{P_4Mo_6\}_2$) cluster, built up from two $[P_4Mo^V{}_6O_{31}]^{12-}$ (abbr. $\{P_4Mo_6\}$) subunits bridged by one metal (M) center, has attracted more attentions due to its specific structure and fascinating physicochemical properties [26–28]. The $\{P_4Mo_6\}$ subunit possesses a high negatively charged surface with all Mo atoms in the +5 oxidation state, which endows the assembled $M\{P_4Mo_6\}_2$ cluster with a peculiar reversible redox feature and makes them an attractive candidate as electrochemical sensor for Cr(VI) detection [29,30]. Importantly, the electron structure of $M\{P_4Mo_6\}_2$ is flexible and tunable, and can be easily manipulated by adjusting the central metal species and the circumjacent functionalized groups, opening up the possibilities for the exploitation of versatile materials with designed functions [31–33]. Nowadays, cadmium oxide as n-type and II–VI semiconductor oxide with a direct and narrow band gap, has arouse increasing interests in the fields of solar cells, phototransistor and photocatalysis [34–38]. Functionalizing hourglass-type $M\{P_4Mo_6\}_2$ cluster with nanosized cadmium oxide cluster will endow the materials with desire photo- and electrochemical activity, thus obtaining efficient detection performance towards trace Cr(VI).

Based on the above consideration, an unusual hexa-nuclear cadmium cluster functionalized reductive phosphomolybdate hybrid with formula of $\{[Cd(H_2O)_2]_2[Cd(btmbp)]_2\}\{Cd(P_4Mo_6O_{31}H_7)_2\}\cdot 20H_2O$ (**1**) (btmbp=4,4′-bis((1*H*-1,2,4-triazol-1-yl)methyl)biphenyl) was hydrothermally synthesized as sensor for photo-assisted electrochemical Cr(VI) detection *via* the reaction of $Na_2MoO_4\cdot 2H_2O$, $CdCl_2\cdot 2.5H_2O$, H_3PO_4 and N-containing btmbp ligand in a C_2H_5OH/H_2O solution at 160 °C (Fig. S1 in Supporting information). Here the closed-shell metal ion Cd^{2+} with $4d^{10}$ configuration was chosen to construct the transition-metal functionalized $M\{P_4Mo_6\}_2$ cluster due to its flexible coordination feature and unique photochemical property. During the hydrothermal synthetic process, the N-containing btmbp ligand and ethanol serve as reducing agent to create a reducing environment for the assembly of the hourglass-type $\{Cd[P_4Mo_6O_{31}H_8]_2\}^{6-}$ cluster (denoted as $Cd\{P_4Mo_6\}_2$). The formed $Cd\{P_4Mo_6\}_2$ cluster with C_3 symmetry can act as structure-directing agent to induce the arrangement of Cd^{2+} into hexa-nuclear ring-shaped Cd-oxo cluster (denoted as $\{Cd_6\}$), thus facilitating the achievement of target $Cd\{P_4Mo_6\}_2$ framework of compound **1**. Meanwhile, for comparison a pure inorganic salt of $Cd\{P_4Mo_6\}_2$ formulated as $K_5[K(H_2O)][Cd(H_2O)_2]_2\{Cd(P_4Mo_6O_{31}H_6)_2\}\cdot 6H_2O$ (**2**) was also synthesized (Table S1 and Fig. S2 in Supporting information).

Single crystal X-ray diffraction analysis demonstrated that compound **1** crystallizes in the space group *C*2/*c* of monoclinic crystal system (Table S1), which is mainly composed of one hourglass-type $Cd\{P_4Mo_6\}_2$ clusters, three kinds of Cd centers and btmbp ligands. In **1**, Cd centers can be divided into three kinds: Cd1, Cd2 and Cd3, respectively. Cd1 serves as sandwiched atom with six-coordinated mode to bridge two $\{P_4Mo_6\}$ subunits into a typical hourglass-type $Cd\{P_4Mo_6\}_2$ cluster with Cd−O bond lengths of 2.250−2.295 Å (Fig. 1a, Tables S2 and S3 in Supporting information). Cd2 and Cd3 centers also display similar six-coordinated octahedral configurations (Fig. 1b), in which Cd2 connects with two opposite μ_2-OH oxygen atoms (O12), two nitrogen atoms from two independent btmbp ligands and two μ_3-O atoms (O25) of two

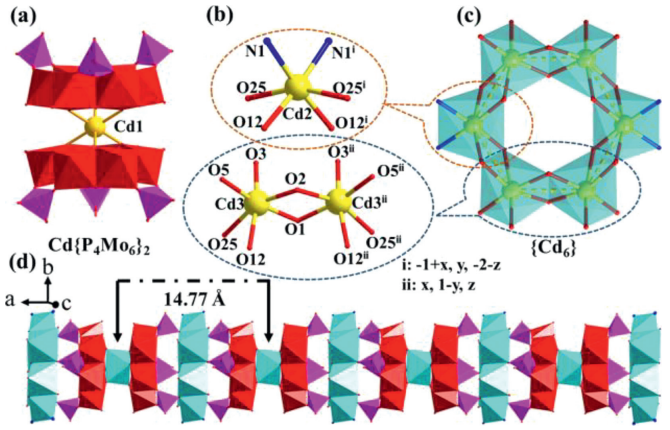

Fig. 1. (a) Polyhedral view of hourglass-type $Cd\{P_4Mo_6\}_2$ cluster in **1**. (b) Coordination environments of three kinds of Cd centers in **1**. (c) Polyhedral view of ring-shaped hexa-nuclear $\{Cd_6\}$ cluster in **1**. (d) 1-D inorganic chain-like structure of **1**. Organic moiety and water molecules were omitted for clarity.

phosphate groups from two $Cd\{P_4Mo_6\}_2$ clusters with Cd-O/N distances of 2.295−2.460 Å, while Cd3-O octahedron is constructed with two μ_2-OH groups (O1 and O12), two μ_3-O-atom donors (O2 and O25) shared with two $\{PO_4\}$ fragments from two different $Cd\{P_4Mo_6\}_2$ clusters and two coordinated water molecules (O3 and O5). It should be noted that two Cd3 centers are linked together *via* the bridging μ_2-OH group (O1) to form a $\{Cd_2\}$ dimer, two sets of $\{Cd_2\}$ dimers are further alternatively coupled with two Cd2 centers to constitute a novel ring-shaped hexa-nuclear $\{Cd_6\}$ cluster (Figs. 1b and c). The non-bonding Cd···Cd contacts in hexa-nuclear ring-like $\{Cd_6\}$ cluster vary from 3.675 Å to 3.756 Å, the angles of ∠Cd3-Cd2-Cd3 and ∠Cd2-Cd3-Cd3 are 119.798° and 120.101°, respectively. Such ring-shaped $\{Cd_6\}$ cluster demonstrated a slightly disordered hexagon character. As shown in Fig. 1d, the $\{Cd_6\}$ subunits in face-to-face mode link $Cd\{P_4Mo_6\}_2$ clusters into one-dimensional (1-D) chain-liked structure of inorganic moiety in **1**. To the best of our knowledge, hexagon $\{Cd_6\}$ cluster has never been reported up to now. As is known that the cadmium clusters display significant role in the various photocatalytic process and the hourglass-type phosphomolybdates have excellent electrochemical properties, the functionalization of the ring-shaped $\{Cd_6\}$ cluster to hourglass-type $Cd\{P_4Mo_6\}_2$ cluster will induce interesting photoelectrochemical properties.

Another significant structural feature of **1** is that the ring-shaped $\{Cd_6\}$ clusters serve as six-connection nodes to coordinate with $Cd\{P_4Mo_6\}_2$ clusters and btmbp ligands to extend the structure into three-dimensional (3-D) porous frameworks (Fig. 2). Concretely, the btmbp ligands with *trans* configuration act as bridging linker to connect with two sets of $\{Cd_6\}$ clusters, and each $\{Cd_6\}$ cluster in 1-D inorganic chain joints with four btmbp ligands. These linkages spread the structure of **1** into a 3-D porous framework with $\{4^{12}.6^3\}$ *pcu* topology (Figs. 2a and b). It is worth noting that there are two kinds of interpenetrating *pcu* nets in such 3-D porous frameworks. The window size of each *pcu* framework is calculated to be 25.69 Å × 25.69 Å, which could be enough to allow another set of network to interwoven it in a parallel manner, resulting in a 2-fold interpenetrating metal–organic network. Owing to this feature, the channel window is divided into four sections with window size of *ca.* 12.85 Å × 12.85 Å (Figs. 2c and d), which could benefit for the mass transport during Cr(VI) detection. These results indicate that hexa-nuclear $\{Cd_6\}$ cluster functionalized reductive $Cd\{P_4Mo_6\}_2$ porous hybrid framework is successfully synthesized. The integration of photoactive $\{Cd_6\}$ subunits with electroactive $Cd\{P_4Mo_6\}_2$ will endow the compound **1** with

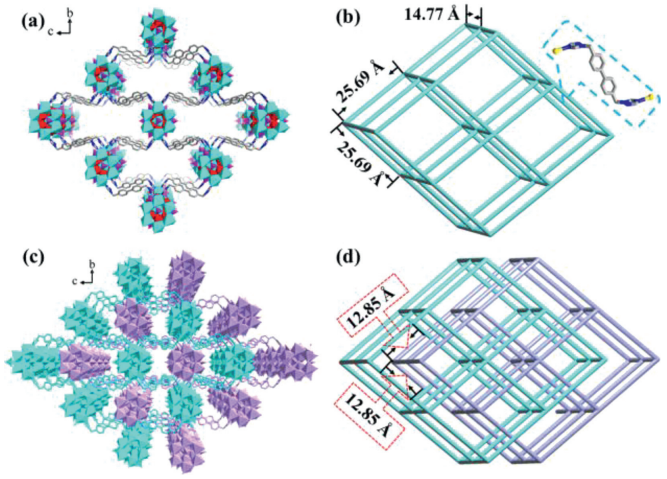

Fig. 2. (a) Ball-and-stick and polyhedral views of the 3-D open framework of **1**. (b) Schematic view of pcu topology framework. (c) The two-fold interpenetrating frameworks in **1**. (d) Schematic topology view of the crystal structure.

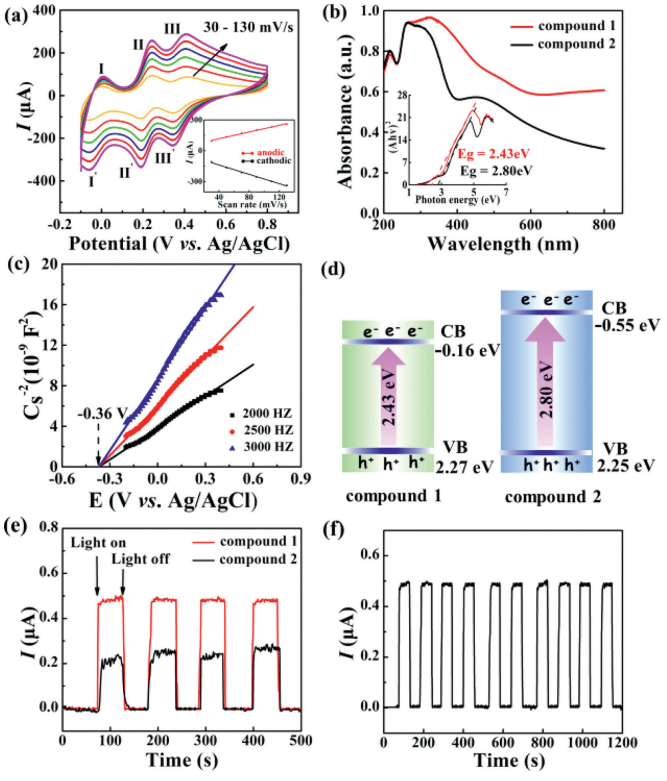

Fig. 3. (a) CV curves of **1** at different scan rates. (b) UV-vis diffuse reflection spectra of **1** and **2**. Insert: the corresponding plot of the $(\alpha h\nu)^2$ *versus* $h\nu$. (c) Mott–Schottky plots of **1** in 0.2 mol/L Na_2SO_4 solution at pH 6.80. (d) Energy diagram of the HOMO and LUMO levels of **1** and **2**. (e) Transient photocurrent response of **1** and **2**. (f) Stability of the transient photocurrent under periodic off-on-off light for 10 cycles.

specific photo-electrochemical properties, making it promising versatile materials toward photo-electrocatalytic reactions.

The structure of **1** was further characterized by Fourier transform infrared spectrum (FT-IR), X-ray powder diffractometer (XRD), thermogravimetric (TG) techniques and Energy dispersive spectrometer (Fig. S3 in Supporting information). Pure inorganic salt of $Cd\{P_4Mo_6\}_2$ cluster named compound **2** was synthesized as comparison (Fig. S4 in Supporting information). The cyclic voltammetry (CV) curves in Fig. 3a show three pairs of redox peaks with half-wave potential $E_{1/2}$ at −26 mV (I-I'), 216 mV (II-II') and 372 mV (III-III') for compound **1**, −15 mV (I-I'), 225 mV (II-II') and 377 mV (III-III') for compound **2** (Table S5 in Supporting information), respectively. They could be ascribed to continuous multi-electrons redox processes of Mo atoms in hourglass-type $Cd\{P_4Mo_6\}_2$ cluster, implying the excellent electrochemical redox property of **1** and **2**. In Fig. 3b, compound **1** exhibits the stronger and wider absorption capacity in the wavelength range of 200∼800 nm compared to compound **2**, indicating that the modification of $\{Cd_6\}$ to $Cd\{P_4Mo_6\}_2$ cluster can promote its optical property. Besides, the band gap (*Eg*) of **1** was measured to be 2.43 eV (Fig. 3b). Mott–Schottky plot of **1** (Fig. 3c) determined the conduction band potential (CB) value of −0.36 V *vs.* Ag/AgCl, which corresponds to −0.16 V *vs.* NHE. The positive slope of the linear region in C^2–E plots reveals the typical n-type semiconductor behavior of **1**. As comparison, the *Eg* of compound **2** is 2.80 eV (Fig. 3b), which is larger than that of **1**, indicating that the functionalization of $\{Cd_6\}$ can regulate the energy band structure of $Cd\{P_4Mo_6\}_2$ cluster. It should be noted that the CB positions of **1** and **2** are more negative than the CB position of Cr(VI)/Cr(III) (+0.51 V, pH 6.8), which signifies the thermodynamically feasibility for the photoreduction Cr(VI) (Fig. 3d and Fig. S5 in Supporting information). In addition, the transient photocurrent response of **1** was measured under visible-light illumination to investigate its photo-induced charges separation efficiency. As depicted in Fig. 3e, compound **1** produced a transient photocurrent of 0.49 μA, showing nearly 2-fold higher than that of compound **2** (0.25 μA). This result suggested that the functionalization of $\{Cd_6\}$ on $Cd\{P_4Mo_6\}_2$ clusters can distinctly accelerate the separation of photo-generated carriers, thereby improving the photoelectrochemical conversion efficiency and amplifying the photocurrents. Moreover, compound **1** displayed stable photocurrents during 10 cycles of on/off light (Fig. 3f), demonstrating great potentials as photoelectrochemical sensors for photo-assisted electrochemical Cr(VI) detection.

The electrochemical performance of title compound for trace Cr(VI) detection was firstly explored in 0.5 mol/L H_2SO_4 electrolyte under dark condition by employing the differential pulse voltammetry (DPV) technique As shown in Figs. 4a and b, the response currents of compound **1** were remarkably enhanced accompanied by the continuous increase of Cr(VI) concentration from 0.1 μmol/L to 1.0 μmol/L, which demonstrates the quick and sensitive electrochemical response abilities of **1** to the change of Cr(VI) concentration. Notably, compound **1** exhibits a benign linear response correlation range in the Cr(VI) concentration from 0.1 μmol/L to 1.0 μmol/L with the linear regression equation of $I(\mu A) = -106.95 \times C(\mu mol/L) - 96.47$, in which C represents the Cr(VI) concentration and I stands for the response current acquired by differential pulse voltammetry (Fig. 4b). Based on the principle of S/N = 3, the detection limit of compound **1** for Cr(VI) is calculated to be 6.25 nmol/L (0.325 ppb) and the sensitivity is 106.95 μA L/μmol, which is superior to **2** and far meets the standard concentration (≤ 0.05 ppm) of WHO set for potable water (Fig. S6 in Supporting information).

To further enhance the detection performance of **1**, the photo-assisted electrochemical Cr(VI) determination was carried out under the illumination of 40 W white light. As shown in Fig. 4c, with addition of 1.0 μmol/L Cr(VI), compound **1** produced a current increment of 196.3 μA, which is apparently larger than that in dark condition (90.6 μA), indicating its excellent photo-electrochemical response. The response current of **1** is also larger than that of compound **2** under the illumination of visible light (Fig. 4c and Fig. S7 in Supporting information), which indicates that the modifying $Cd\{P_4Mo_6\}_2$ cluster with $\{Cd_6\}$ cluster can promote their photoactivity and accelerate the electron transfer process during Cr(VI) detection, thus achieving distinct response signal. Moreover, with the continuous addition of Cr(VI), the DPV curves of compound **1** (Figs. 4d and e) demonstrated a distinct linear re-

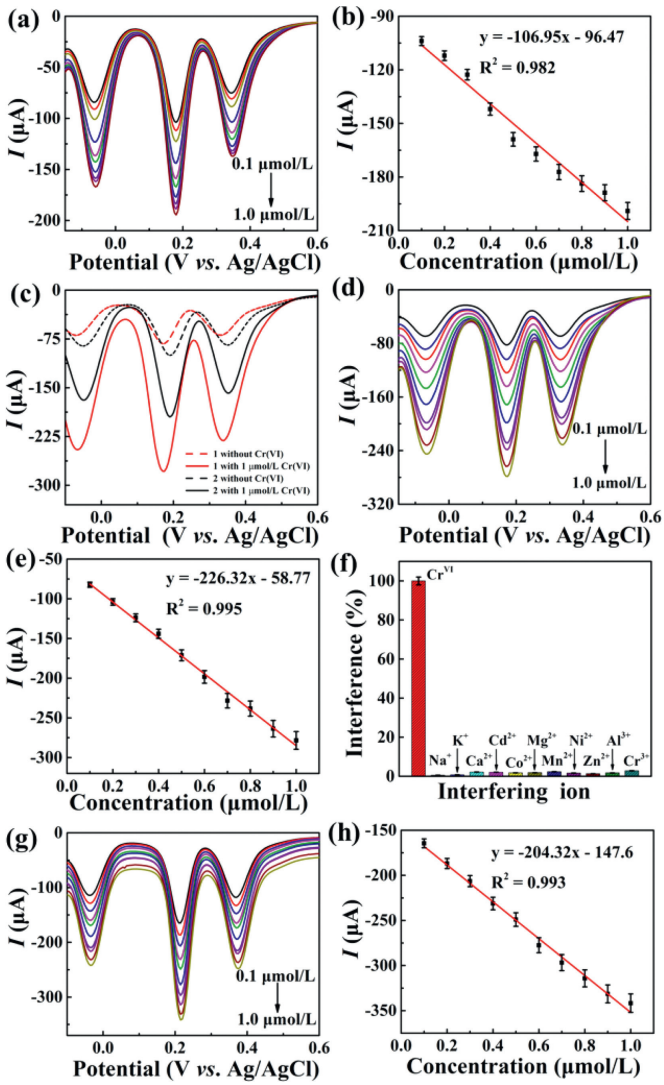

Fig. 4. (a) DPV curves of compounds **1**-modified electrodes in 0.5 mol/L H_2SO_4 with continuous addition of Cr(VI). (b) Its corresponding linear dependences of **1**. (c) DPV curves of **1** and **2** in 0.5 mol/L H_2SO_4 with the addition of 1.0 μmol/L Cr(VI) under visible light illumination. (d) DPV curves of **1** with continuous additions of Cr(VI) under the visible light illumination. (e) The linear dependence curve of **1**; (f) Current interference of **1** towards Cr(VI) with different interferents of 400 μmol/L Na^+, K^+, Ca^{2+}, Cd^{2+}, Co^{2+}, Mg^{2+}, Mn^{2+}, Ni^{2+}, Zn^{2+}, Al^{3+}, $Cr^{3+}$and their mixture with 40 μmol/L Cr(VI), respectively. (g) DPV curves of compound **1** in acidified lake water with continuous additions of Cr(VI). (h) The linear dependence curve of **1.**

lationship range with the linear regression equations of $I(\mu A) = -226.32 \times C(\mu mol/L) - 58.77$ ($R^2 = 0.995$), from which the LODs of compound **1** were calculated to be 4.17 nmol/L (0.225 ppb) and the sensitivity is as high as 226.32 μA L/μmol. Compared to the dark condition, the sensitivity of compound **1** enhanced from 106.95 to 226.32 μA L/μmol and the Cr(VI) LODs improved from 6.25 to 4.17 nmol/L, manifesting the excellent photo-electrochemical detection activity of **1** towards Cr(VI). Such performance far meets the requirements of WHO set for drinking water (50 ppb) and superior to most of reported noble metal-based electrochemical sensors (Table S6 in Supporting information). To gain more insights, the electrochemical impedance spectroscopy (EIS) was used to study the electron transfer behavior of **1** in dark and light-irradiation condition. As shown in Fig. S8 (Supporting information), compound **1** exhibits a small electron transfer resistance under irradiation, revealing its fast electron-transfer capacity and excellent photoactivity. In addition, in order to further exclude the impact of organic ligand on the detection performance, the DPV of btmbp ligand was also investigated, which show that there is nearly no detection performance towards Cr(VI) (Fig. S9 in Supporting information). Besides, the analytic selectivity and anti-interference of **1** was examined by adding some common metal ions (Na^+, K^+, Ca^{2+}, Cd^{2+}, Co^{2+}, Pb^{2+}, Mg^{2+}, Mn^{2+}, Ni^{2+}, Zn^{2+}, Al^{3+}, Cr^{3+}) into the Cr(VI) detection system, respectively. It can be found from Fig. 4f that only the introduction of Cr(VI) can engender evident response current signal and the impact of these interference ions on response current does not exceed 3%. These results suggest that compound **1** possesses great anti-interference capacity and high selectivity to Cr(VI), which provides a basis for heavy metal Cr(VI) detection in practical aqueous environmental system.

Then, compound **1** was employed as photoelectrochemical sensor to determine the Cr(VI) concentration in the real lake water sample. As shown in Figs. 4g and h, compound **1** displayed apparent response current towards Cr(VI) with the linear regression equation of $I(\mu A) = -204.32 \times C(\mu mol/L) - 147.6$ ($R^2 = 0.993$), from which the sensitivity and detection of limit of **1** were calculated to be 204.32 μA L/μmol and 4.73 nmol/L (0.246 ppb), respectively. This result not only satisfies the standard of WHO, also shows good conformity with that in deionized water, implying the significant practicability of **1**. Moreover, compound **1** exhibited good long-term durability and it can continuously operate in Cr(VI)-containing 0.5 mol/L H_2SO_4 electrolyte for 10 h with slight change of the signal currents (Fig. S10 in Supporting information), suggesting the excellent electrocatalytic stability of compound **1**. In addition, the structural stability of compound **1** after electrochemical detection was also characterized. Fig. S11 (Supporting information) shows the IR and XRD patterns of compound **1** after electrochemical detection. It was found that all peak positions almost remained unchanged, revealing its excellent structural stability. These results further illustrate the great promise of compound **1** for practical implications of Cr(VI) detection in environmental system.

In summary, an unusual hexa-nuclear cadmium cluster functionalized reductive phosphomolybdate sensor was synthesized for photo-assisted electrochemical detection of ultra-trace Cr(VI) in real samples. With the help of photo-assistance, compound **1** displayed efficient photo-assisted electrochemical Cr(VI) detection performance with the Cr(VI) LOD of 4.17 nmol/L (0.225 ppb) and sensitivity of 226.32 μA L/μmol, which is apparently superior to the performance without photo-assistance (6.25 nmol/L and 106.95 μA L/μmol) and far satisfies the demands of WHO set for potable water (50 ppb). This work provides an efficient avenue for designing efficient POM-based crystalline materials for photoelectrochemical reactions.

Declaration of competing interest

The authors declare that they have no known competing financial interest or personal relationships that could have appeared to influence the work reported in this paper.

Acknowledgments

This work is supported by the National Natural Science Foundation of China (Nos. 21871076, 21901060), Natural Science Foundation of Hebei Province (Nos. B2016205051, B2020205008 and B2019205074), Science and Technology Project of Hebei Education Department (No. BJ2020037), Project funded by China Postdoctoral Science Foundation (No. 2021TQ0095), the Science Foundation of Hebei Normal University (No. L2019B15).

Supplementary materials

Supplementary material associated with this article can be found, in the online version, at doi:10.1016/j.cclet.2021.12.021.

References

[1] Y. Xu, T.Q. Wang, Z.D. He, et al., Chem. Eur. J. 24 (2018) 14436–14441.
[2] L. Cui, J. Wu, H.X. Ju, Chem. Eur. J. 21 (2015) 11525–11530.
[3] B. Shen, C. Dong, J. Ji, et al., Chin. Chem. Lett. 30 (2019) 2205–2210.
[4] Z.X. Ren, X.J. Liu, Z.H. Zhuge, et al., Chin. J. Catal. 41 (2020) 180–187.
[5] Y. Zhao, Y. Sun, Y. Jiang, et al., Sci. China Chem. 62 (2019) 133–141.
[6] Q. Yang, H. Wang, F. Li, et al., J. Mater. Chem. A 9 (2021) 13306–13319.
[7] J.J. Pang, R.H. Du, X. Lian, et al., Chin. Chem. Lett. 9 (2021) 13306–13319.
[8] Y. Mao, S. Gao, L. Yao, et al., J. Hazard. Mater. 408 (2021) 124898.
[9] L.H. Chen, X.B. Cai, Q. Li, et al., J. Solid State Chem. 302 (2021) 122416.
[10] Q.W. Bao, G. Li, Z.C. Yang, et al., Chin. Chem. Lett. 31 (2020) 2752–2756.
[11] M.H. Motaghedifard, S.M. Pourmortazavi, S. Mirsadeghi, Sens. Actuators. B: Chem. 327 (2021) 128882.
[12] M.M. Ahmeda, R.H. Zhao, B. Hayytova, et al., Chin. Chem. Lett. 31 (2020) 2091–2094.
[13] L. Saghatforousha, M. Hasanzadeh, N. Shadjou, Chin. Chem. Lett. 25 (2014) 655–658.
[14] C. Yuan, H. Gao, Q. Xu, et al., Appl. Surf. Sci. 521 (2020) 146431.
[15] S. Hu, Y. Yu, Y. Guan, et al., Chin. Chem. Lett. 31 (2020) 2839–2842.
[16] Y. Xu, J. Han, Y. Luo, et al., Adv. Funct. Mater. 31 (2021) 2105001.
[17] Y. Si, A.Y. Zhang, C. Liu, et al., Water Res. 157 (2019) 30–39.
[18] S. Hu, Y. Wei, J. Wang, et al., Anal. Chim. Acta 1178 (2021) 338793.
[19] X. Tian, Y. Zhang, Y. Ma, et al., Catal. Sci. Technol. 10 (2020) 2593–25601.
[20] L.Z. Qiao, M. Song, A.F. Geng, et al., Chin. Chem. Lett. 20 (2019) 1273–1276.
[21] Y.-W. Peng, C. Shan, H.J. Wang, et al., Adv. Energy Mater. 9 (2019) 1900597.
[22] Y.T. Song, Y.W. Peng, S. Yao, et al., Chin. Chem. Lett. 33 (2022) 1047–1050.
[23] H. Sun, H.Q. Yin, W. Shi, et al., Nano Res. 15 (2022) 3026–3033.
[24] N. Zhang, L.Y. Hong, A.F. Geng, et al., Chin. Chem. Lett. 29 (2018) 1409–1412.
[25] M. Zhao, X.Y. Zhu, Y.Z. Li, et al., Tungsten 4 (2022) 121–129.
[26] G.P. Yang, K. Li, X.L. Lin, et al., Chin. J. Chem. 39 (2021) 3017–3022.
[27] D.Y. Du, J.S. Qin, T.T. Wang, et al., Chem. Sci. 3 (2012) 705–710.
[28] G.P. Yang, Y.F. Liu, K. Li, et al., Chin. Chem. Lett. 31 (2020) 3233–3236.
[29] X. Xin, N. Hu, Y.Y. Ma, et al., Dalton Trans. 49 (2020) 4570–4577.
[30] J.Q. Niu, W.T. An, X.J. Zhang, et al., Chem. Eng. J. 418 (2021) 129408.
[31] G.P. Yang, X.L. Zhang, Y.F. Liu, et al., Inorg. Chem. Front. 8 (2021) 4650–4656.
[32] H. Zhang, K. Yu, J. Li, et al., RSC Adv. 5 (2015) 3552–3559.
[33] M.T. Lv, Y.F. Liu, K. Li, et al., Tetrahedron Lett. 65 (2021) 152757.
[34] W.H. Wang, T. Lu, L.H. Liu, et al., J. Hazard. Mater. 419 (2021) 126464.
[35] M. Burbano, D.O. Scanlon, G.W. Watson, J. Am. Chem. Soc. 133 (2011) 15065–15072.
[36] X. Tang, H.F. Lu, Q.Y. Zhang, et al., Solid State Sci. 13 (2011) 384–387.
[37] S.F.J. Cox, J.S. Lord, S.P. Cottrell, et al., J. Phys. Condens. Mat. 18 (2006) 1061–1078.
[38] B.K. Balachandar, T. Logu, R.H. Ramprasath, et al., Mater. Sci. Semicond. Proc. 105 (2020) 104753.